Turn-on Solid-State Fluorescent determination of Zinc Ion by Quinoline-based Covalent Organic Framework

*Paloma García-Arroyo[1], Elena Gala[1,2], Marcos Martínez-Fernández[1], Elena Salagre[3,4], José I. Martínez[5], Enrique G. Michel[3,4] and José L. Segura[1]**

P. García Arroyo, E. Gala, M. Martínez-Fernández, J.L. Segura
[1]Departamento de Química Orgánica I, Facultad de CC. Químicas, Universidad Complutense de Madrid, 28040 Madrid, Spain.
E-mail: segura@ucm.es

E. Gala
[2]Chemical and Environmental Technology Department, Rey Juan Carlos University, Móstoles, 28933, Spain.

E. Salagre, E. G. Michel
[3]Departamento de Física de la Materia Condensada, Universidad Autónoma de Madrid, 28049, Madrid, Spain
[4]Condensed Matter Physics Center (IFIMAC), Universidad Autónoma de Madrid, 28049, Madrid, Spain.

J.I. Martínez
[5]Departamento de Materiales de baja dimensionalidad, Instituto de Ciencia de Materiales de Madrid (ICMM-CSIC),28049 Madrid, Spain

Keywords: covalent organic framework, Povarov reaction, Zn ion determination

A new quinoline-based COF, obtained by Povarov reaction, containing 2,6-diisopropylphenyl moieties as substituents over the heterocyclic ring is described for detecting Zn^{2+} in aqueous solution. The introduction of the mentioned bulky phenyl rings into the network favors an increase of the distance between the reticular sheets and their arrangement, obtaining a new material with an alternating AB type stacking. The new

material exhibits good selectivity to detect Zn^{2+} by fluorescence emission in aqueous solutions up to a concentration of 1.2×10^{-4} M of the metal ion. In order to have a deeper insight into the interaction between the COF and the zinc cation, a thorough spectroscopical, microscopical and theoretical study is also presented and discussed in this communication.

1. Introduction

Selective and sensitive recognition of metal ions (e.g., Hg, Cd, Fe, Al, Cu, etc.) is a field of increasing scientific interest. In particular, fluorescent sensing has attracted growing significance due to its simplicity, high sensitivity and outstanding selectivity, and it has been applied for a wide range of applications.[1–3] Thus, different metal ions can be detected by spectroscopic changes of fluorescence-based sensory materials, which also allow low-cost and real-time assays.[4,5]

In the past few years, Covalent Organic Frameworks (COFs) have emerged as new promising porous crystalline materials with potential applications in multiple fields, since they display ordered extended structures, low density, high porosity, tunable pore surface (size and shape), etc.[6–8] Furthermore, their high specific surface area and the π-stacked layered structure enable the formation of defined paths within the framework, favoring the interaction with the suitable analytes and also enhancing the sensitivity through signal amplification. In addition, engineering the pore surface can further optimize the diffusion of complementary analytes.[9–11] Based on these convenient features, COFs have outcome as novel potential fluorescent probes for the detection of biologically and environmentally valuable analytes, specially metal ions.[12–16]

Zinc is the second most abundant transition metal ion in the human body. It is also involved in several essential biological processes of all living organisms such as cell growth and apoptosis, DNA binding and synthesis, gene transcription, immune function, etc.[17–20] However, the excess or lack of the proper amount of zinc ion in the body can cause acute health problems.[21,22] In case of Zn deficiency, severe chronic liver and renal diseases, digestion problems or mental retardation can be generated.[23,24] In contrast, neurotoxicity and the development of neurodegenerative diseases (like Parkinson or Alzheimer) are related to an excess Zn ion concentration in some cells.[25] Besides its diverse biological roles, Zinc is also an important transition metal in the environment and industry; several agricultural and industrial products use Zinc, since it protects steel from oxidation and corrosion.[26] Due to its unique properties, it is of big interest the selective

and sensitive detection of Zn metal ions.[27–30] In this regard, several analytical and electrochemical techniques.[31–35] have been applied for the recognition of metal ions, specifically Zn^{2+}. However, most of those methods need sample pre-treatment and/or have high-cost and low selectivity. In addition, Zn detection is specially challenging due to its electron configuration ($3d^{10}4s^{0}$), which hinders any spectroscopic or magnetic response.[36,37] For these reasons, in recent years there has been growing interest in the development of novel fluorescence chemosensors, since their simple and precise method of detection has outcome as a promising alternative to conventional analytical methods. Moreover, fluorescence chemosensors can be further applied to bioimaging.[38]

Up to now, several Zn^{2+} sensors based on quinoline, anthracene, fluorescein, coumarin, BODIPY or Schiff bases have been reported.[39–44] Among those, quinoline moieties and its derivatives have outstand due to their specific selectivity towards Zn^{2+} with a "turn-on" fluorescent enhancement that potentially improve the sensitivity of the material.[44–47] Thus, utilization of quinoline as an efficient fluorescence sensor towards metal ions has shown great promise and potential.

As it has been mentioned above, COFs have been successfully applied for the sensing of different metal ions, including Cu^{2+}, Hg^{2+}, Au^{+}. Fe^{3+} and Pb^{2+}.[2,48,49] However, and for the best of our knowledge, no previous applications of COFs as fluorescent detectors of Zn^{2+} have been reported. Thus, it is of big interest the development of novel COF-based fluorescence platforms for "turn-on" fluorescence detection of Zn^{2+}.

In this contribution, starting from imine-based COF, we describe the successful transformation into more robust and conjugated 2D aromatic network (**Quin-COF**). While certain crystallinity and porosity are preserved, the chemical and thermal stability plus the π-electron delocalization in the resultant quinoline-linked COF is enhanced. The as-obtained quinoline-COF was further studied as a potential "turn-on" selective fluorescent detector of Zn metal ions.

2. Results and discussion

2.1. Synthesis and characterization of Quin-COF

The efficient aza-Diels-Alder (azaDA) reaction between the aryl imines of the **TAPB-DMTP-COF**[50] and the alkyne group of the arylalkyne derivative affords the conversion of the dynamic imine linkage into more stable quinoline-linked **Quin-COF** (Scheme 1).

Due to the potential chemical tunability of the substrates in the cycloaddition reaction, different functionalities can be introduced within the pores of the COFs frameworks in a post-synthetic approach.[51] In this work, 2,6-diisopropylphenyl moieties were integrated onto the pores. While the 2D COF displays strong covalent bonds along the plane, weak van der Waals forces direct the interactions along the out-of-plane direction. For this reason, the introduction of this bulky pendant groups within the layered framework will hinder the π-π interaction between layers, enhancing surface/functional group accessibility for further analytes facile diffusion in sensing applications.[52,53]

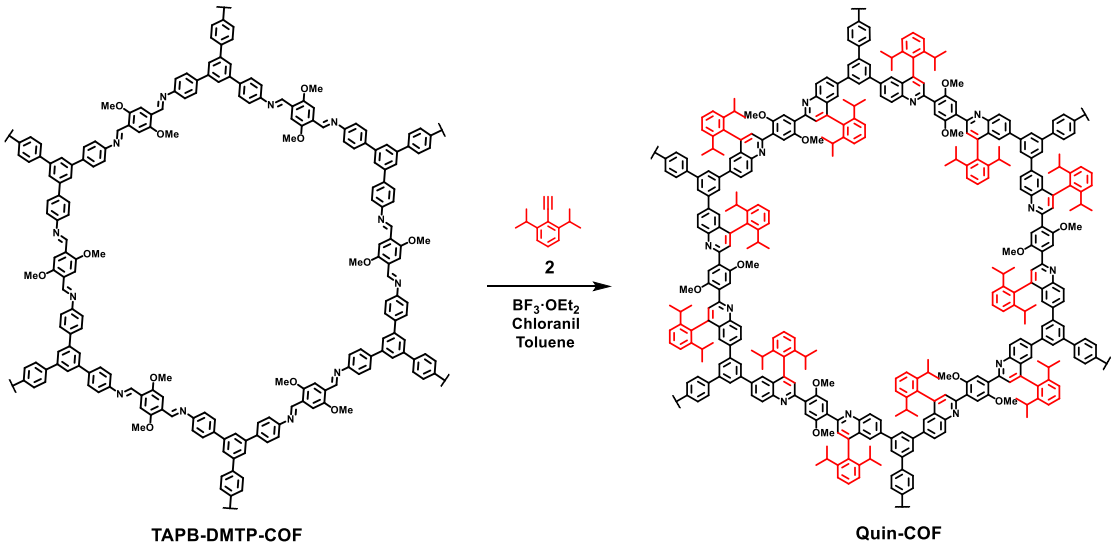

Scheme 1. Synthesis of **Quin-COF** via aza-Diels-Alder cycloaddition reaction.

The fruitful incorporation of the bulky 2,6-diisopropylphenylacetylene onto the pristine **TAPB-DMTP-COF** was confirmed by Fourier transform infrared spectroscopy (FT-IR). The comparative spectra of the powders **TAPB-DMTP-COF** and **Quin-COF** (**Figure 1a**) revealed an emergence band at 1681cm^{-1}, attributed to the stretch of aromatic quinoline core. Furthermore, the spectrum shows the presence of the characteristic C(sp^3)-H stretching band from the 2,6-diisopropylphenyl moieties at 2975 cm^{-1}.

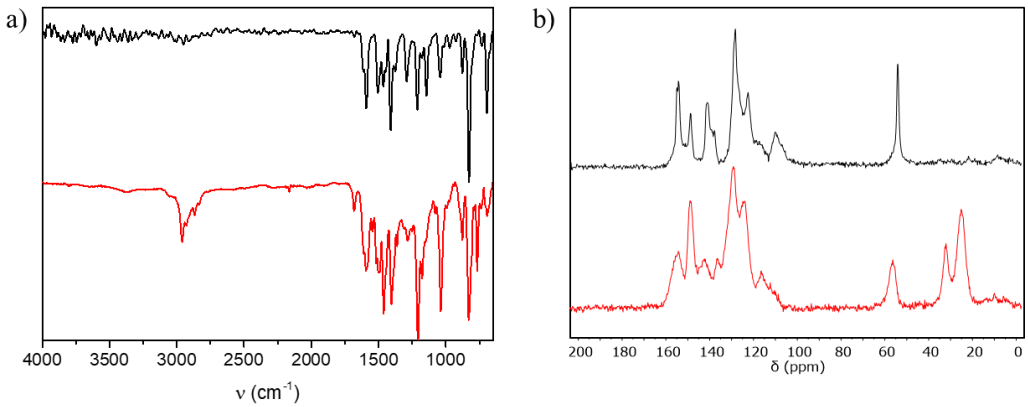

Figure 1. a) ATR-FTIR spectra of **TAPB-DMTP-COF** (black) and **Quin-COF** (red). b) ^{13}C NMR of **TAPB-DMTP-COF** (black) and **Quin-COF** (red).

The solid state ^{13}C cross polarization magic angle spinning NMR (^{13}C-CP/MAS NMR) spectrum of **Quin-COF** shows two signals at 32.51 and 25.10 ppm, successfully assigned to the sp^3 C of the 2,6-diisopropylphenyl units (**Figure 1b**). In addition, a slight down-field shift of the signals corresponding to the aromatic -OMe substituents is observed in the spectrum of **Quin-COF** in comparison with that corresponding to **TAPB-DMTP-COF** (from 56.39 ppm to 55 ppm, respectively). Due to the enhanced aromaticity in the resulting network, the aromatic signals in the carbon spectrum are more intense and wider compared to the initial COF aromatic signals (Figure 1b).

Crystallinity analysis of the linkage-transformed COFs was performed by powder X-ray diffraction (PXRD). As it is shown in **Figure 2**, backbone modification leads to a crystalline domains reduction as reported in other quinoline based COFs modified by Povarov´s reaction,[54,55] or imine to tiocarbamate chemical modification.[56] In this way, the pore size reduction by the introduction of the bulky 2,6-diisopropylphenyl moieties shifts the original (100) diffraction maxima from 2.90º to 3.35º, respectively, according to de Bragg´s law.

N_2 sorption isotherms at 77 K (**Figure S1a**) revealed a Brunauer−Emmett−Teller (BET) surface area of 2166 and 144.18 $m^2\ g^{-1}$ for **TAPB-DMTP-COF** and **Quin-COF**, respectively. A total pore volume of 1.22, and 0.13 $cm^3\ g^{-1}$ was derived in each case. The reduction of surface area and pore volume is in good agreement with the increased framework mass and the introduction of the aromatic phenyl pendant rings. Both

materials exhibited a type IV isotherm, indicating the mesoporous characters, with a pore size distribution centered at 2.6 and 2.1 nm for **TAPB-DMTP-COF** and **Quin-COF** (**Figure S1b**), respectively, calculated by non-local density functional theory (NLDFT).

The significant changes observed in crystallinity, surface areas and pore volume between **TAPB-DMTP-COF** and **Quin-COF** would be explained in terms of changes in stacking: The introduction of the voluminous diisopropylphenyl fragments into the pore would provoke the displacement of COF sheets, going from an eclipsed AA to an alternated AB stacking. In order to have a deeper knowledge about the stacking of the new material **Quin-COF**, a comprehensive series of DFT calculations were conducted (see SI for detailed information). The simulations resulted in both **TAPB-DMTP-COF** and **Quin-COF** 2D structures featuring canonical hexagonal P6 symmetry, each exhibiting monolayer lattice parameters of 37.21 and 37.34 Å, respectively. **TAPB-DMTP-COF** adopts a preferential eclipsed (AA) stacking configuration, maintaining a consistent π–π stacking interlayer distance of 3.58 Å. In contrast, **Quin-COF** exhibits highly inefficient interlayer stacking due to the out-of-plane conformation of the 2,6-diisopropylphenyl ligand moieties, which forms an angle of 90 degrees with the plane of the skeleton COF, resulting in a theoretically predicted interlayer distance of 6.42 Å (see **Figure 2**). The corresponding diffractograms, simulated based on these optimized structures, demonstrate excellent agreement with experimental evidence, thereby affirming the validity of the structures derived from simultaneous structure + cell DFT geometrical optimizations.

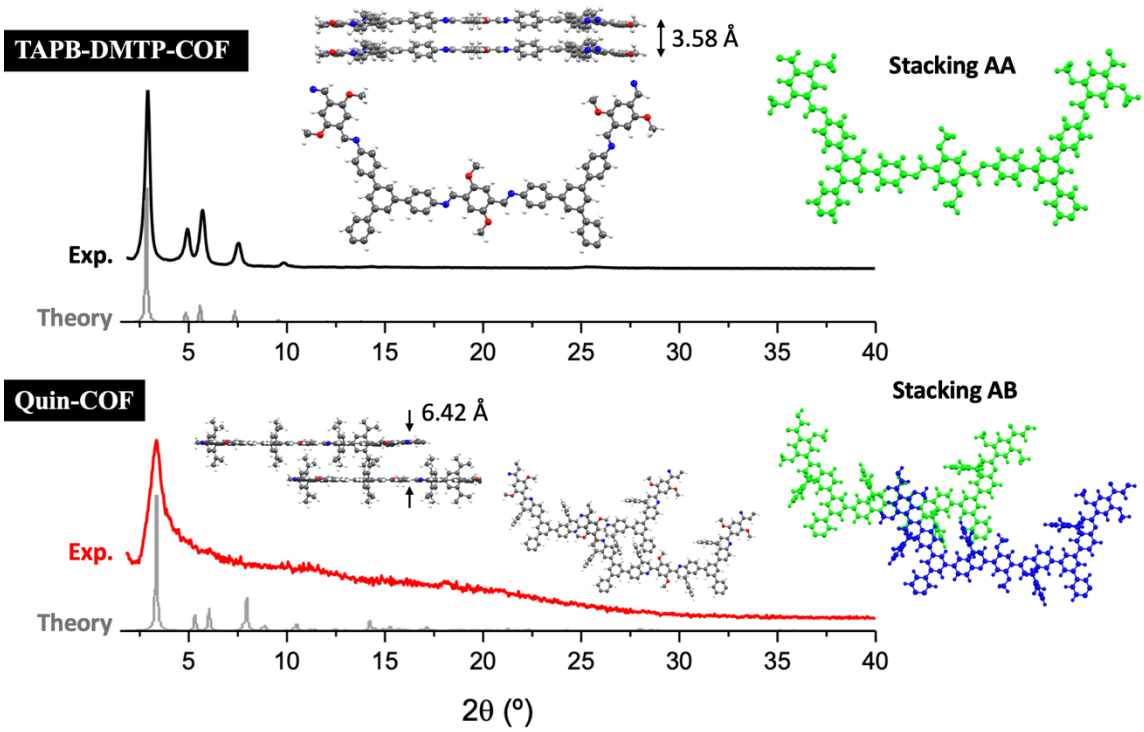

Figure 2. Experimental and simulated diffractograms obtained from the resulting DFT-optimized structures for the **TAPB-DMTP-COF** and **Quin-COF** systems. Top and side pictorial views of the DFT-optimized crystal-bulk structures are shown, indicating interlayer distances and preferential stacking configurations.

Comparison between UV-Vis spectra of initial product **TAPB-DMTP-COF** and resulting material **Quin-COF** (**Figure S2**) showed a significant bathochromic shift in the absorbance as a result from the enhanced π delocalization of the polymeric networks. The enhancement of the aromaticity and electron delocalization was also evidenced in the thermal stability of **Quin-COF**, studied by thermogravimetric analysis (TGA), revealing that the new material has a higher decomposition onset temperature compared to its respective precursor **TAPB-DMTP-COF** (**Figure S3**).

X-ray electron spectroscopy (XPS) was performed to determine the conversion of the reaction. As it can be observed in **Figure S4**, the N1*s* peak corresponding to the imine nitrogen of **TAPB-DMTP-COF** was identified at ~398.5 eV,[54] together with residual contributions that could be attributed to rests of oxidized nitrogen. The transformation of **TAPB-DMTP-COF** into **Quin-COF** was evidenced in the XPS by an increase in a high binding energy component of the N 1*s* peak associated with quinoline groups (Figure S4).

The analysis of the peak area allowed us to determine that the degree of conversion of imine groups into quinoline moieties was a 20%.

Additionally, scanning electron microscopy (SEM) was conducted for the two materials, suggesting that not significant changes in the morphology occurred after the chemical transformation (**Figure 3a and 3b**). Furthermore, the layered structure of the 2D **Quin-COF** could be observed by transmission electron microscopy (TEM, **Figure 3c and 3d**).

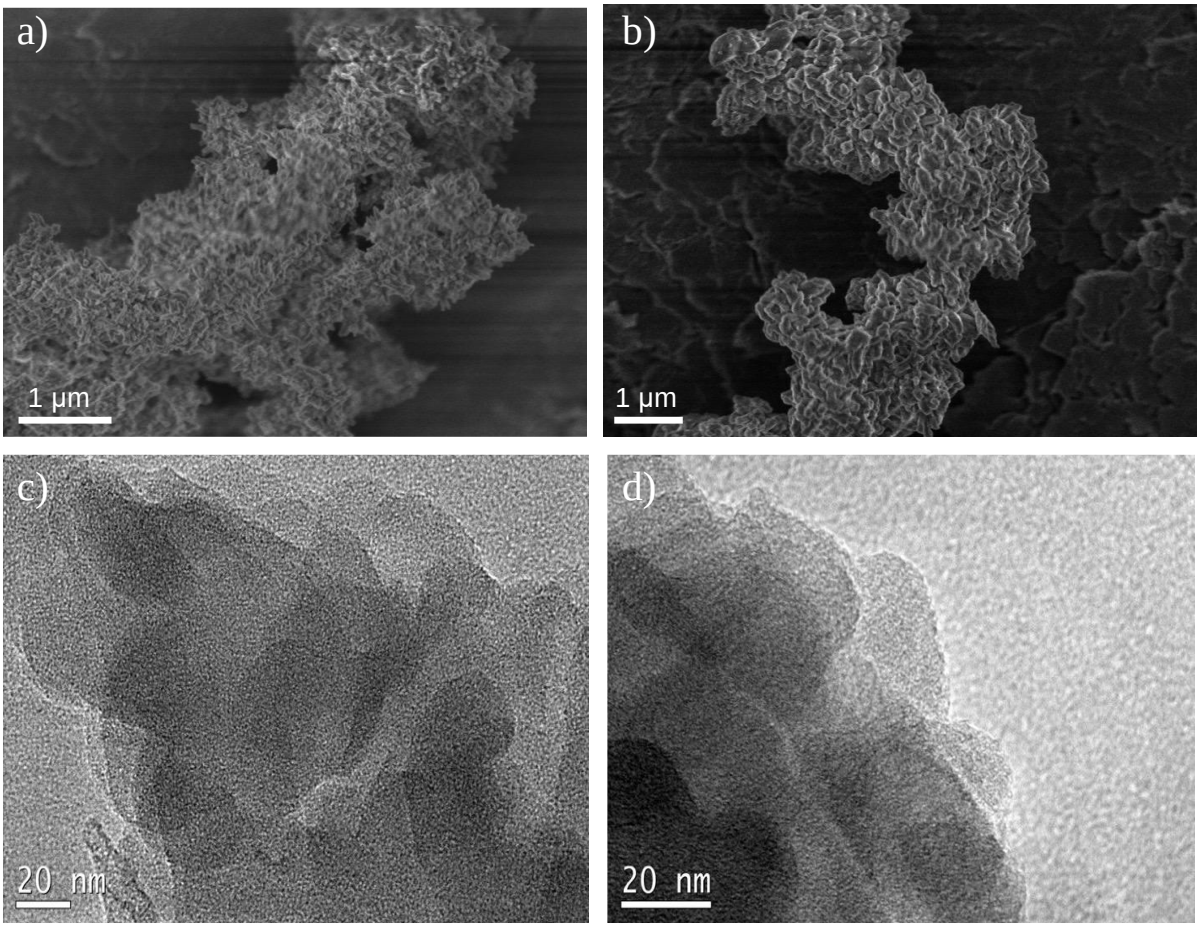

Figure 3. SEM images of (a) **TAPB-DMTP-COF**, (b) **Quin-COF**. (c,d) TEM images of **Quin-COF**.

2.2. Fluorescence studies

Fluorescence spectroscopy was used to study the fluorescent properties of the synthesized COF. Upon excitation at λ_{ex} = 450 nm, inconspicuous fluorescence was observed for all materials (**Figure 4**). The maximum emission band appeared at 520 nm for **TAPB-DMTP-COF**, while the corresponding one for **Quin-COF** appeared at 500 nm.

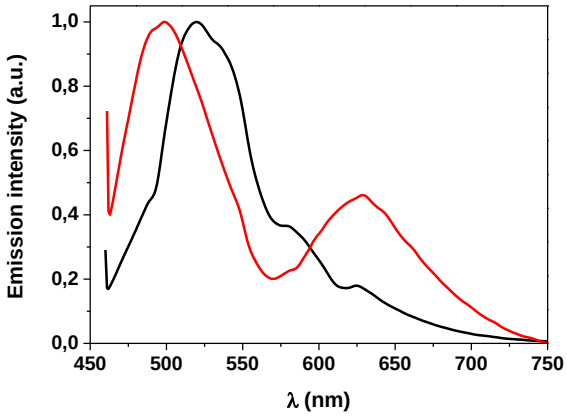

Figure 4. Fluorescence spectra of **TAPB-DMTP-COF** (black) and **Quin-COF** (red) dispersed in a mixture of THF:H_2O (1:1) (λ_{ex} = 450 nm).

However, the incorporation of quinoline moieties in the resulting framework motivated the study of the material as selective detector of Zn^{2+} by monitoring real-time fluorescence changes upon increasing Zn^{2+} concentrations. Thus, **Quin-COF** was ultrasonically dispersed (35 kHz, 80W, 30 min, RT) in a mixture of THF:H_2O (1:1) at a concentration of 0.08 mg·mL^{-1} and further sonicated for 5 min. The fluorescence titrations were performed by systematically increasing the concentration of Zn^{2+} in the cuvette (from $1x10^{-5}$ M until $2x10^{-4}$ M) and subsequent record of the fluorescence intensity. For all the measurements, the excitation wavelength was λ_{ex} = 450 nm and the corresponding emission wavelength was recorded from λ_{em}= 460-750 nm. As shown in **Figure 5**, the fluorescence intensity of **Quin-COF** is boosted upon increasing concentrations of Zn^{2+}, indicating a real-time "turning on" mechanism and reaching its maximum at [Zn^{2+}] = $1.2x10^{-4}$ M.

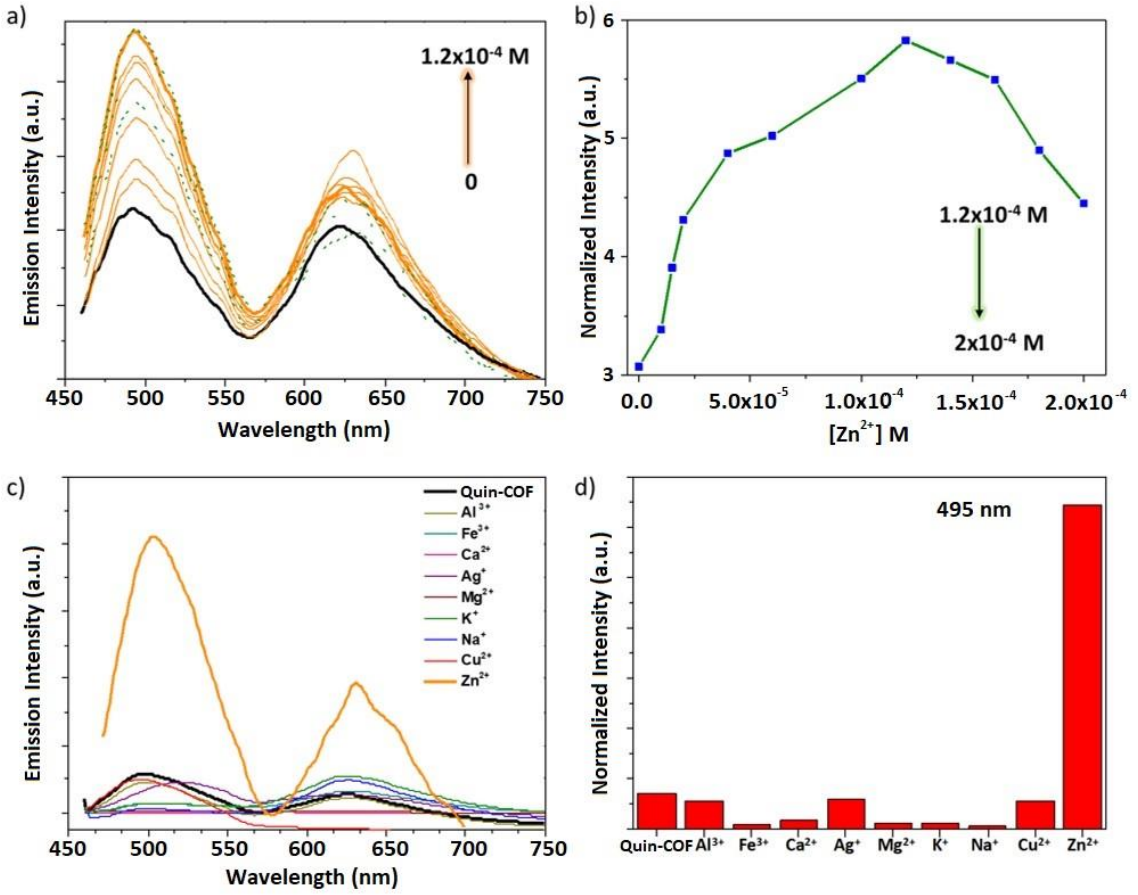

Figure 5. a) Fluorescence spectra of **Quin-COF** (black, 0.08 mg mL^{-1}) dispersed in THF:H_2O (1:1) containing increasing concentrations of Zn^{2+} (Orange, λ_{ex}=450 nm). b) Normalized fluorescence intensity of **Quin-COF** dispersion (0.08 mg mL^{-1}) upon increasing concentrations of Zn^{2+} (λ_{ex}=450 nm). c) Selective binding of **Quin-COF** to Zn^{2+} ion. The fluorescence spectra of **Quin-COF** dispersed in THF:H_2O (1:1) upon addition of 0.15 M of different metal ions (λ_{ex}=450 nm); d) Fluorescence intensity of **Quin-COF** in THF:H_2O (1:1) dispersion at 510 nm in the presence of different metal ions (λ_{ex}=450 nm); [**Quin-COF**] = 0.05 mg·mL^{-1}; [metal ion] = 0.15 M.

The selectivity of **Quin-COF** towards Zn^{2+} was then studied by detecting the fluorescence intensity change in the presence of different metal ions at equal concentrations. In particular, Al^{3+}, Fe^{3+}, Ca^{2+}, Ag^{+}, Mg^{2+}, K^{+}, Na^{+}, Cu^{2+} and Zn^{2+} were added to dispersed solutions of **Quin-COF** (0.08 mg·mL^{-1}). The corresponding fluorescence spectra of **Quin-COF** after adding different metal ions were illustrated in Figure 5. Remarkably, due to the Zn specific metal binding property of **Quin-COF**, only the presence of Zn^{2+} in the solution turned-on the fluorescence emission. Even though all fluorescence spectra of metal ions-COF dispersions were measured under the same conditions, a clear selectivity

towards Zn^{2+} could be observed, displaying strong emission while the other dispersions had a negligible emission. These results further support the great selectivity of this material as a potential chemosensor for the detection of Zn^{2+}.

2.3. Study of interaction of Zn^{2+} with Quin-COF

Due to the great number of active sites on the COF skeleton, Zn^{2+} could effectively bound to the quinoline moieties, which leads to the fluorescence on/off mechanism. This metal ion-COF interaction was confirmed by dispersing **Quin-COF** in THF:H_2O (1:1) solution of Zn metal ions. The resulting **Zn@Quin-COF** was analyzed by scanning electron microscopy (SEM) and energy-dispersive X-ray spectroscopy (EDX) (**Figure 6**), confirming the successful incorporation of the Zn^{2+} to the COF framework.

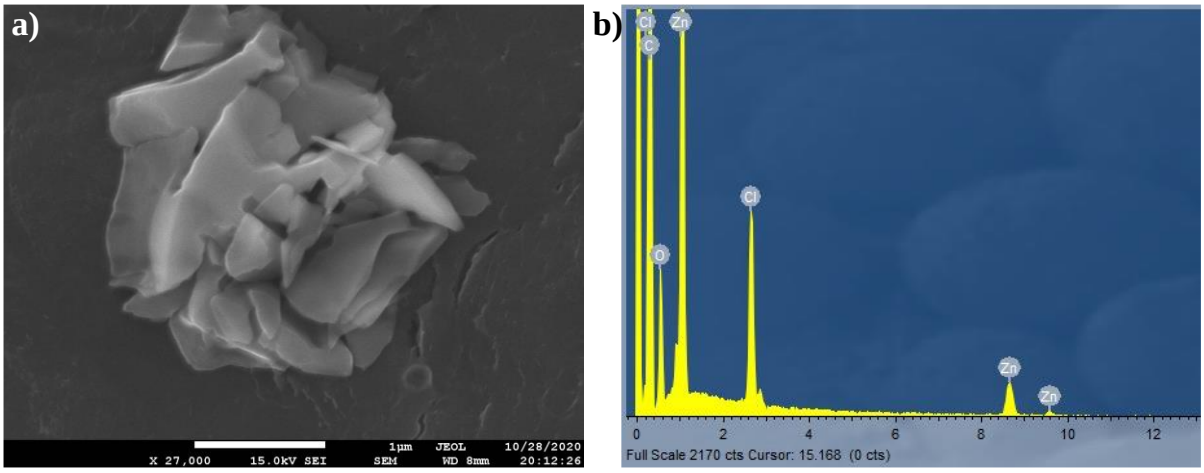

Figure 6. (a) SEM micrograph of **Zn@Quin-COF** and (b) EDX spectra of **Zn@Quin-COF** sample revealing the presence of atomic Zn in the complexed structures.

The successful introduction of Zn^{2+} into the network was also evidenced with an exhaustive XPS study of **Zn@Quin-COF**. Most notable observation was noticed at N 1*s* peak, in which a shift to a higher binding energy (~ 0.5±0.1 eV) with respect **Quin-COF** was recorded. This change is associated with the loss of electronical density over the nitrogen atom due to its proximity to the positive charged metal ion. No shifting was observed in signals corresponding to C 1*s* and O 1*s*, so interaction between Zn^{2+} and the COF seems to occur only through the nitrogen atom. Direct visualization of Zn^{2+} resulted challenging because of the low intensity of the Zn signals, which were observed very shifted, approximately 15 eV for Zn 3*p* and 3*s*, while the signal corresponding to Zn 2*p* is barely perceptible (**Figure S5**). We hypothesize that the shifting observed in the Zn

core level peaks may be due to charge accumulation effects during the measurement process because interaction between **Quin-COF** and Zn^{2+} are weak and not enough to allow effective shielding of the gap created during the photoemission process. The succesful introduction of Zn in the network is proven by the emergence of Zn 3*p* and 3*s* signals in **Zn@Quin-COF** XPS spectra, in contrast to their absence in the original **Quin-COF** compound. The region corresponding to the Zn 2*p* (330-350 eV of kinetic energy) has a similar appearance, due to the presence of the O KLL Auger peak (Figure S5a). An estimate of the Zn/N ratio through the light cores Zn 3*p* and N 1*s* using their effective sections, gives a ratio of 0.44 (Zn/N).

The interaction between Zn^{2+} and **Quin-COF** though nitrogen atoms was also corroborated with theoretical studies. Once the structure of **Quin-COF** compound was established, we explored, following the same theoretical protocol afore-explained (see SI for detailed information), different possibilities towards the stabilization of Zn^{2+} ions within the COF structure. For that purpose, we studied the anchoring of a Zn atom on a large variety of adsorption sites within **Quin-COF**. Among all the possibilities analyzed, just two Zn-complexation configurations were particularly stable compared to the rest of conformations investigated (**Figure 7**). The two most stable Zn-adsorption configurations are: i) an "Out-of-plane" configuration (Figure 7a); where the Zn-ion is located on top a six-membered C-ring with an average distance between the Zn and the C-atoms of around 3.05 Å and an adsorption energy of 0.17 eV, and ii) a "Coplanar" configuration, the most stable one (Figure 7b); where the Zn-ion is side-interacting with the structure located coplanar to the quinoline plane, with the shortest distances to the neighboring H atoms and N atom of 2.36, 2.66 and 3.06 Å, respectively, and an adsorption energy of 0.25 eV, around a 30% higher than in the previous configuration. This theoretical finding excellently agrees with the experimental XPS evidence, which yields a clear interaction of the Zn-ions with the quinoline units within the **Quin-COF**.

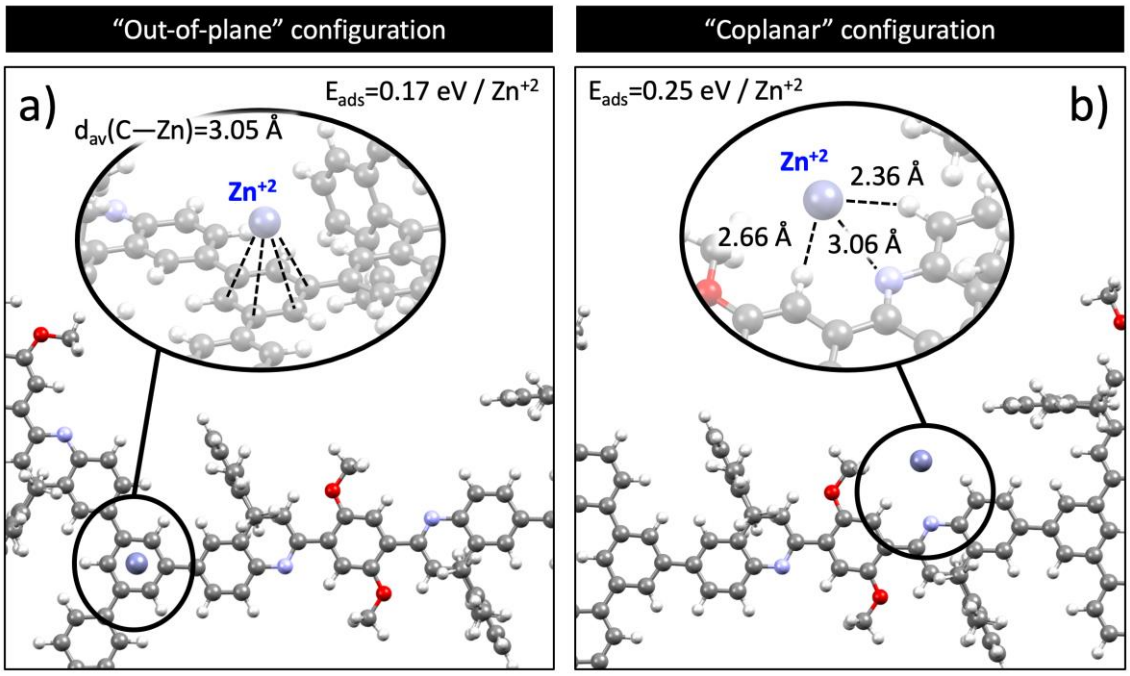

Figure 7. DFT-optimized geometries corresponding to the two most stable Zn^{+2} adsorption sites within the **Quin-COF** structure: a) "Out-of-plane" configuration; where the Zn-ion is located on top a six-membered C-ring, and b) "Coplanar" configuration; where the Zn-ion is side-interacting with the structure located coplanar to the quinoline plane. Representative distances and adsorption energy for the Zn-ion are also indicated for each configuration.

In order to evaluate the differences in the optical properties of the different pristine **TAPB-DMTP-COF** and **Quin-COF** compounds, and of the complexed **Zn@Quin-COF** in its most stable "coplanar" configuration, we have computed the TD-DFT UV-Vis absorption spectra of molecular fragments representative of all these systems within the main purpose to rationalize the potential "turn-on" selective **Quin-COF** chemosensor towards Zn metal-ions experimentally proposed. The representative molecular fragments considered are shown in **Figure 8** for the **TAPB-DMTP-COF** and **Quin-COF** compounds, and of the complexed **Quin-COF** with 1 and 2 adsorbed Zn atoms. In the case with two Zn atoms, they are located in the most stable adsorption configurations side-interacting with the two quinoline units in the fragment. The TDDFT-computed UV–Vis absorption spectra in Figure 8 exhibits their most important optical absorption features below 550 nm. For the case of the **TAPB-DMTP** fragment we only find a sharp excitation above 350 nm at around 370 nm (labelled as transition **1**), which after the electronic decay will yield a poor fluorescence signal, as observed in the experiments. On

the contrary, for the other three cases Quin, Quin@1Zn and Quin@2Zn, this wavelength region up to 450 nm shows a richer optical absorption signal scenario and a clear bathochromic shift in the absorbance as a result from the enhanced π delocalization. Besides, the Quin-based molecular fragments introduce a novel feature in the absorption spectra at around 460 nm (labelled as transition **2**) with refence to the **TAPB-DMTP** system, which will enhance the fluorescent signal after electronic decay, in excellent agreement with the experimental observations.

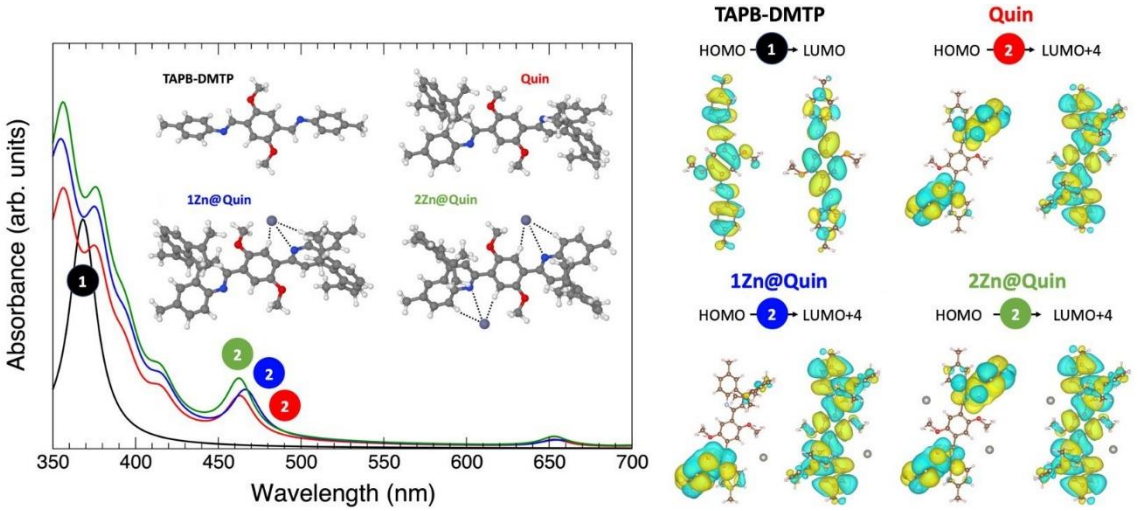

Figure 8. TDDFT-computed UV–Vis absorption spectra of the molecular fragments representative of the **TAPB-DMTP-COF**, **Quin-COF**, and **1Zn@Quin-COF** and **2Zn@Quin-COF** in THF:water (1:1). Optimized geometries of the molecular fragments and most relevant related electronic transitions are also shown.

Specifically, theoretical calculations predict that transition **1** in **TAPB-DMTP** occurs between the HOMO and LUMO states. These states possess distinct yet compatible electronic character, enabling the permitted transition. Interestingly, these states are distributed throughout the fragment structure. On the other hand, the electronic origin of Transition **2** in Quin- fragments differs. This absorption feature at 460 nm originates consistently from the HOMO, with its destination state being LUMO+4 in all cases. Notably, there is no significant wavelength shift for this feature, irrespective of the Zn-complexation degree. However, there is an increase in absorption intensity as the number of complexing-Zn atoms increases from 0 to 2, with a roughly 15% intensity enhancement

from 0 to 1 and from 1 to 2 Zn atoms. This observation underscores the system's potential as a selective chemosensor for Zn metal ions.

An examination of the morphology of the HOMO and LUMO+4 states within these fragments reveals that the HOMO state is associated with the 2,6-diisopropylphenyl moieties. In the cases of **Quin** and **Quin@2Zn**, the HOMO is symmetrically located on both ligands simultaneously due to the high symmetry of the systems. In contrast, for the **Quin@1Zn** fragment, the unbalanced geometrical symmetry manifests in the electronic structure. The 2-fold degenerate HOMO in the previous fragments splits into two states, each located in one of the 2,6-diisopropylphenyl ligands. The LUMO+4 state is consistently located throughout the entire fragment in all cases. It is noteworthy that the Zn-complexation effect breaks the HOMO electronic symmetry and induces optical absorption enhancement not only for Transition 2 but also across the entire region up to 450 nm. This phenomenon may stem from Zn-complexation inducing a rigidification of certain bonds, impeding the dissipation of absorbed energy across the structure and enabling enhanced absorption and emission signatures within the visible range.

3. Conclusion

In conclusion, we have successfully synthesized a robust quinoline-linked covalent organic framework (**Quin-COF**) by simple transformation of the dynamic imine linkages of readily available **TAPB-DMTP-COF** via aza-Diels-Alder reaction, which enabled the integration of 2,6-diisopropylphenyl pendant rings onto the pore surface. The incorporation of quinoline moieties and bulky pendant groups within the pores of the polymer favored the change of stacking between the layers, obtaining a material with an alternated AB stacking. The sensing experiments towards metal ions have been performed, funding an excellent selective “turn-on” fluorescence emission towards Zn^{2+} ions. The XPS, microscopical and theoretical studies corroborated the interaction between the **Quin-COF** and Zn^{2+} through quinoline ring.

4. Experimental Section

Details of synthesis, purification and characterization of **2** and **DMTP-TAPB-COF** are provided in Supporting Information.

Synthesis of ***Quin-COF***. **Quin-COF** was synthesized by following a previously reported procedure based on Povarov reaction with slightly modifications.[57] **TPB-DMTP-COF** (100 mg), 2,6-diisopropylphenylacetylene **2** (233 mg, 1.25 mmol), $BF_3{\cdot}OEt_2$ (100 μL, 0.75 mmol), chloranil (200 mg, 0.75 mmol) and toluene (50 mL) were added to an ace pressure tube. The tube was sealed and heated under argon at 110 °C for 3 days. After the reaction time, the mixture was cooled to room temperature and the precipitate was filtered. The reaction mixture was then washed with THF and quenched with saturated aqueous Na_2CO_3. The resulting precipitate was washed with H_2O, Soxhlet extracted with THF and dried under vacuum at 120 °C, yielding **Quin-COF** as a yellow solid (200 mg, quantitative). ^{13}C NMR (100 MHz, ss-CP/MAS, δ): 154.31, 148.93, 142.53, 136.72, 129.20, 124.83, 115.99, 56.39, 32.51, 25.10. FTIR (ATR) ϑ (cm^{-1}): 2964, 2857, 1681, 1582, 1545, 1461, 1410, 1402, 1208, 1180, 1038, 876, 835, 774. PXRD 2θ (°): 3.35, 11.36, 18.12, 20.65, 28.43.

Supporting Information

Supporting Information is available from the Wiley Online Library or from the author.

Acknowledgements

The authors are fully acknowledged for financial support from the Spanish Ministry of Science and Innovation MICINN (Grants TED2021-129886B-C43, PID2022-138908NB-C33, PID2021-123295NB-I00, PID2020-113142RB-C21, PLEC2021-007906 and TED2021-129416A-I00). JLS, PGA, EG and MMF also acknowledge funding from Universidad Complutense de Madrid, (INV.GR.00.1819.10759). EGM and ES acknowledge financial support from the Spanish Ministry of Science and Innovation, through the "María de Maeztu" Programme for Units of Excellence in R&D (CEX2018-000805-M). JIM also acknowledges funding from Comunidad de Madrid (Grants S2018/NMT-4367 and Y2020/NMT-6469).

Received: ((will be filled in by the editorial staff))
Revised: ((will be filled in by the editorial staff))
Published online: ((will be filled in by the editorial staff))

References

[1] K.P. Carter, A.M. Young, A.E., Palmer *Chem. Rev.* **2014**, *114*, 4564–4601. https://doi.org/10.1021/cr400546e.

[2] J. Zhang, F. Cheng, J. Li, J.-J. Zhu, Y. Lu *Nano Today*. **2016**, *11*, 309–329. https://doi.org/10.1016/j.nantod.2016.05.010.

[3] Y. Liu, Q. Ouyang, H. Li, M. Chen, Z. Zhang, Q. Chen *J. Agric. Food Chem.* **2018**, *66*, 6188–6195. https://doi.org/10.1021/acs.jafc.8b00546.

[4] M. Vendrell, D. Zhai, J.C. Er, Y.-T. Chang *Chem. Rev.* **2012**, *112*, 4391–4420. https://doi.org/10.1021/cr200355j.

[5] B. Kaur, N. Kaur, S. Kumar *Coord. Chem. Rev.* **2018**, *358*, 13–69. https://doi.org/10.1016/j.ccr.2017.12.002.

[6] Y. Liu, X. Liu, A. Su, C. Gong, S. Chen, L. Xia, C. Zhang, X. Tao, Y. Li, Y. Li, T. Sun, M. Bu, W. Shao, J. Zhao, X. Li, Y. Peng, P. Guo, Y. Han, Y. Zhu *Chem. Soc. Rev.* **2023**, 502–544. https://doi.org/10.1039/d3cs00287j.

[7] K.T. Tan, S. Ghosh, Z. Wang, F. Wen, D. Rodríguez-San-Miguel, J. Feng, N. Huang, W. Wang, F. Zamora, X. Feng, A. Thomas, D. Jiang *Nat. Rev. Methods Prim.* **2023**, *3*, 1. https://doi.org/10.1038/s43586-022-00181-z.

[8] J. Martín-Illán, D. Rodríguez-San-Miguel, F. Zamora *Coord. Chem. Rev.* **2023**, *495*,. https://doi.org/10.1016/j.ccr.2023.215342.

[9] X. Zhang, G. Li, D. Wu, B. Zhang, N. Hu, H. Wang, J. Liu, Y. Wu *Biosens. Bioelectron.* **2019**, *145*, 111699. https://doi.org/10.1016/j.bios.2019.111699.

[10] W. Huang, Y. Jiang, X. Li, X. Li, J. Wang, Q. Wu, X. Liu *ACS Appl. Mater. Interfaces*. **2013**, *5*, 8845–8849. https://doi.org/10.1021/am402649g.

[11] A.P. Côté, A.I. Benin, N.W. Ockwig, M. O'Keeffe, A.J. Matzger, O.M. Yaghi *Science* **2005**, *310*, 1166 – 1170. https://doi.org/10.1126/science.1120411.

[12] X. Liu, D. Huang, C. Lai, G. Zeng, L. Qin, H. Wang, H. Yi, B. Li, S. Liu, M. Zhang, R. Deng, Y. Fu, L. Li, W. Xue, S. Chen *Chem. Soc. Rev.* **2019**, *48*, 5266–5302. https://doi.org/10.1039/C9CS00299E.

[13] C. Xing, Y. Zhang, D. Wei, Y. Zhi *Macromol. Rapid Commun.* **2024**, *2300678*, 1–8. https://doi.org/10.1002/marc.202300678.

[14] M. Wang, Y. Qin, Z. Li, Z. Song, Y. Wan, J. Du, M. Song, S. Li, S. Zhang, M. Zhao *Trends Anal. Chem.* **2024**, *172*, 117589. https://doi.org/10.1016/j.trac.2024.117589..

[15] K. Xu, N. Huang *Chem. Res. Chinese Univ.* **2022**, *38*, 339–349. https://doi.org/10.1007/s40242-022-1476-4.

[16] J. Liu, J. Wang, Y. Wang, Y. Wang *J. Polym. Sci.* **2022**, *n/a*,. https://doi.org/10.1002/pol.20220683.

[17] P. Mazumdar, S. Maity, D. Das, S. Samanta, M. Shyamal, A. Misra *Sensors Actuators B Chem.* **2017**, *238*, 1266–1276. https://doi.org/10.1016/j.snb.2016.09.084.

[18] M. Patil, K. Keshav, M.K. Kumawat, S. Bothra, S.K. Sahoo, R. Srivastava, J. Rajput, R. Bendre, A. Kuwar *J. Photochem. Photobiol. A Chem.* **2018**, *364*, 758–763. https://doi.org/10.1016/j.jphotochem.2018.07.015.

[19] T. Mandal, A. Hossain, A. Dhara, A. Al Masum, S. Konar, S.K. Manna, S.K. Seth, S. Pathak, S. Mukhopadhyay *Photochem. Photobiol. Sci.* **2018**, *17*, 1068–1074. https://doi.org/10.1039/c8pp00186c.

[20] B. Chen, P. Yu, W.N. Chan, F. Xie, Y. Zhang, L. Liang, K.T. Leung, K.W. Lo, J. Yu, G.M.K. Tse, W. Kang, K.F. To *Signal Transduct. Target. Ther.* **2024**, *9*, 6. https://doi.org/10.1038/s41392-023-01679-y.

[21] J.L. Domingo *J. Toxicol. Environ. Health*. **1994**, *42*, 123–141. https://doi.org/10.1080/15287399409531868.

[22] R. Eisler. Zinc Hazards to Fish, Wildlife, and Invertebrates: A Synoptic Review, Laurel, MD, 1993, iv, 106.

[23] D. Maity, T. Govindaraju *Chem. Commun.* **2012**, *48*, 1039–1041. https://doi.org/10.1039/c1cc16064h.

[24] X. Chen, C.S. Lim, D. Lee, S. Lee, S.J. Park, H.M. Kim, J. Yoon *Biosens. Bioelectron.* **2017**, *91*, 770–779. https://doi.org/10.1016/j.bios.2017.01.042.

[25] Z. Li, Y. Liu, R. Wei, V.W. Yong, M. Xue *Biomolecules*. **2023**, *13*, 1–15. https://doi.org/10.3390/biom13010028.

[26] A. Kalendová, P. Kalenda, D. Veselý *Prog. Org. Coatings*. **2006**, *57*, 1–10. https://doi.org/10.1016/j.porgcoat.2006.05.015.

[27] Z.M. Dong, W. Wang, L.Y. Qin, J. Feng, J.N. Wang, Y. Wang *J. Photochem. Photobiol. A Chem.* **2017**, *335*, 1–9. https://doi.org/10.1016/j.jphotochem.2016.11.014.

[28] W. Wang, R. Li, T. Song, C. Zhang, Y. Zhao *Spectrochim. Acta Part A Mol. Biomol. Spectrosc.* **2016**, *164*, 133–138. https://doi.org/10.1016/j.saa.2016.04.016.

[29] S. Dey, A. Roy, G.P. Maiti, S.K. Mandal, P. Banerjee, P. Roy *New J. Chem.* **2016**, *40*, 1365–1376. https://doi.org/10.1039/C5NJ02723C.

[30] S.Y. Park, J.H. Yoon, C.S. Hong, R. Souane, J.S. Kim, S.E. Matthews, J. Vicens

J. Org. Chem. **2008**, *73*, 8212–8218. https://doi.org/10.1021/jo8012918.

[31] S. Mandal, Y. Sikdar, D.K. Maiti, R. Sanyal, D. Das, A. Mukherjee, S.K. Mandal, J.K. Biswas, A. Bauzá, A. Frontera, S. Goswami *J. Photochem. Photobiol. A Chem.* **2017**, *334*, 86–100. https://doi.org/10.1016/j.jphotochem.2016.10.038.

[32] J.S. Ganesan, S. Gandhi, K. Radhakrishnan, A. Balasubramaniem, M. Sepperumal, S. Ayyanar *Spectrochim. Acta Part A Mol. Biomol. Spectrosc.* **2019**, *219*, 33–43. https://doi.org/10.1016/j.saa.2019.04.029.

[33] Y. Liu, P. Liu, S. Liu, Y. Guo, H. He, C. Yang, J. Song, N. Zhang, J. Cheng, Z. Chen *J. Clin. Virol.* **2018**, *101*, 29–33. https://doi.org/10.1016/j.jcv.2018.01.015.

[34] B.-Y. Kim, H.-S. Kim, A. Helal *Sensors Actuators B Chem.* **2015**, *206*, 430–434. https://doi.org/10.1016/j.snb.2014.09.071.

[35] G.A. Antunes, H.S. dos Santos, Y.P. da Silva, M.M. Silva, C.M.S. Piatnicki, D. Samios *Energy & Fuels*. **2017**, *31*, 2944–2950. https://doi.org/10.1021/acs.energyfuels.6b03360.

[36] N. Narayanaswamy, T. Govindaraju *Sensors Actuators B Chem.* **2012**, *161*, 304–310. https://doi.org/10.1016/j.snb.2011.10.036.

[37] L. Chen, T. Lou, C. Yu, Q. Kang, L. Chen *Analyst*. **2011**, *136*, 4770–4773. https://doi.org/10.1039/C1AN15585G.

[38] J. Yu, H. Yu, S. Wang, Y. Qi *J. Lumin.* **2024**, *266*, 120318. https://doi.org/10.1016/j.jlumin.2023.120318.

[39] H.G. Lee, B.K. Kim, G.J. Park, Y.J. Na, H.Y. Jo, S.A. Lee, C. Kim *Inorg. Chem. Commun.* **2014**, *39*, 61–65. https://doi.org/10.1016/j.inoche.2013.10.049.

[40] K. Chantalakana, N. Choengchan, P. Yingyuad, P. Thongyoo *Tetrahedron Lett.* **2016**, *57*, 1146–1149. https://doi.org/10.1016/j.tetlet.2016.01.106.

[41] S. Mizukami, S. Okada, S. Kimura, K. Kikuchi *Inorg. Chem.* **2009**, *48*, 7630–7638. https://doi.org/10.1021/ic900247r.

[42] H. He, D.K.P. Ng *Chem. – An Asian J.* **2013**, *8*, 1441–1446. https://doi.org/10.1002/asia.201300183.

[43] V. Gupta, A. Singh, L. Kumawat *Sensors Actuators B Chem.* **2014**, *204*, 507–514. https://doi.org/10.1016/j.snb.2014.07.128.

[44] A. Kim, H. Lee, D. Yun, U. Jung, K.-T. Kim, C. Kim *Spectrochim. Acta Part A Mol. Biomol. Spectrosc.* **2020**, *241*, 118652. https://doi.org/10.1016/j.saa.2020.118652.

[45] B. Zhang, H. Liu, F. Wu, G. Hao, Y. Chen, C. Tan, Y. Tan, Y. Jiang *Sensors*

Actuators B Chem. **2017**, *243*, 765–774. https://doi.org/10.1016/j.snb.2016.12.067.

[46] Y. Chen, L. Zhao, J. Jiang *Spectrochim. Acta Part A Mol. Biomol. Spectrosc.* **2017**, *175*, 269–275. https://doi.org/10.1016/j.saa.2016.12.034.

[47] S. Sinha, B. Chowdhury, N.N. Adarsh, P. Ghosh *Dalt. Trans.* **2018**, *47*, 6819–6830. https://doi.org/10.1039/C8DT00611C.

[48] G. Chen, H.-H. Lan, S.-L. Cai, B. Sun, X.-L. Li, Z.-H. He, S.-R. Zheng, J. Fan, Y. Liu, W.-G. Zhang *ACS Appl. Mater. Interfaces*. **2019**, *11*, 12830–12837. https://doi.org/10.1021/acsami.9b02640.

[49] Y. Cao, R. Wu, Y.Y. Gao, Y. Zhou, J.J. Zhu *Nano-Micro Lett.* **2024**, *16*, 1–28. https://doi.org/10.1007/s40820-023-01249-5.

[50] H. Xu, J. Gao, D. Jiang *Nat. Chem.* **2015**, *7*, 905–912. https://doi.org/10.1038/nchem.2352.

[51] E. Gala, M.M. Ramos, J.L. Segura *Encyclopedia*. **2023**, *3*, 795–807. https://doi.org/10.3390/encyclopedia3030057.

[52] S. Haldar, K. Roy, R. Kushwaha, S. Ogale, R. Vaidhyanathan *Adv. Energy Mater.* **2019**, *9*, 1902428. https://doi.org/10.1002/aenm.201902428.

[53] S. Kim, H.C. Choi *ACS Omega*. **2020**, *5*, 948–958. https://doi.org/10.1021/acsomega.9b03549.

[54] X. Li, C. Zhang, S. Cai, X. Lei,V. Altoe, F. Hong, J.J. Urban, J. Ciston, E.M. Chan, Y. Liu *Nat. Commun.* **2018**, *9*, 2998. https://doi.org/10.1038/s41467-018-05462-4.

[55] Y. Liang, M. Xia, Y. Zhao, D. Wang, Y. Li, Z. Sui, J. Xiao, Q. Chen *J. Colloid Interface Sci.* **2022**, *608*, 652–661. https://doi.org/10.1016/j.jcis.2021.09.150.

[56] S.J. Lyle, T.M. Osborn Popp, P.J. Waller, X. Pei, J.A. Reimer, O.M. Yaghi *J. Am. Chem. Soc.* **2019**, *141*, 11253–11258. https://doi.org/10.1021/jacs.9b04731.

Table of contents entry.

This communication shows the synthesis and characterization of a quinoline-based COF containing bulky pendant phenyl rings as substituents, distinguished by an alternate AB stacking. This new material has been tested as fluorescent detector, observing selectivity for the detection of Zn^{2+}. A thoughtful characterization has been accomplished to determine the type of interaction between the COF and the Zn^{2+}.

Paloma García-Arroyo, Elena Gala, Marcos Martínez-Fernández, Elena Salagre, José I. Martínez, Enrique G. Michel and José L. Segura*

Turn-on Solid-State Fluorescent determination of Zinc Ion by Quinoline-based Covalent Organic Framework

ToC figure